Colloids and Surfaces A: Physicochemical and Engineering Aspects 672 (2023) 131763

Contents lists available at ScienceDirect

Colloids and Surfaces A: Physicochemical and Engineering Aspects

journal homepage: www.elsevier.com/locate/colsurfa

Trojan-like doxorubicin and gold nanoparticle entrapped smart nanostructured lipid carriers for breast cancer synergistic chemo/photothermal therapy

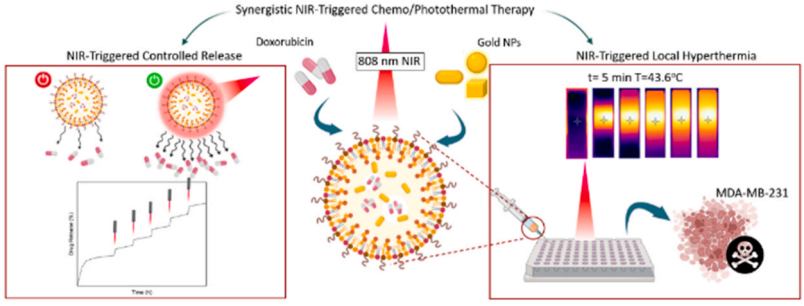
Cigdemnaz Ersoz Okuyucu [a], Gokce Dicle Kalaycioglu [a], Demet Kacaroglu [b], Ayse Kevser Ozden [b], Nihal Aydogan [a,*]

[a] Hacettepe University, Department of Chemical Engineering, Beytepe, 06800 Ankara, Turkey
[b] Lokman Hekim University, Faculty of Medicine, Medical Biology Department, Ankara, Turkey

HIGHLIGHTS

- NLCs were used as a drug delivery system as well as a Trojan for gold Nanoparticles.
- NIR responsive release of drug was achieved.
- These NLCs can be used as a Synergistic therapy Agent.

GRAPHICAL ABSTRACT



ARTICLE INFO

Keywords:
Nanostructured lipid carriers
Gold nanoparticles
Photothermal therapy
Breast cancer

ABSTRACT

Breast cancer is one of the fatal diseases renowned worldwide. Chemotherapy is not sufficient for the treatment of breast cancer in a significant number of cases. In this study, we present the doxorubicin (DOX) and gold nanoparticles (AuNPs) loaded nanostructured lipid carriers (DOX+AuNPs)@NLCs, designed for dual chemo/photothermal therapy. Different geometries of AuNPs (gold nanospheres (AuNSs), gold nanorods (AuNRs), and gold nanocubes (AuNCs)) were also loaded in NLCs to exploit their photothermal heating capacity and to conceptualize the most efficient combination of drug delivery system for combined therapy. The light-triggered on-demand release of DOX from NLCs was examined before and after NIR irradiation (808 nm). The highest heating potential was obtained via AuNRs with $\Delta T = 22\ ^{\circ}C$ in 5 min with 19.5 μg Au/mg lipid. The cytotoxic effect of these formulations was evaluated on MDA-MB-231 breast cancer cells and the highest growth inhibition (81%) is achieved with (DOX+AuNRs)@NLC under 5 min NIR application. It is found that the geometry directly effects the photothermal capability of AuNPs, a synergistic interaction between cytotoxic action of DOX and local hyperthermia provided by AuNPs can significantly enhance the skills on the irreversible cellular damage and developed state-of-art formulations hold a great potential as a combined-cancer-therapy agent. Thus, this study offers promise for the development of a lipid-based nano-platform that is biocompatible, multifunctional, and can be utilized for combined therapy, with tunable properties.

* Corresponding author.
E-mail address: anihal@hacettepe.edu.tr (N. Aydogan).

https://doi.org/10.1016/j.colsurfa.2023.131763
Received 24 April 2023; Received in revised form 11 May 2023; Accepted 28 May 2023
Available online 30 May 2023
0927-7757/© 2023 Elsevier B.V. All rights reserved.

1. Introduction

Cancer is a significant global health issue and ranks as the second most common cause of death [1]. When looking at the distribution of the cancer cases, it was reported that the first most common type is breast cancer globally. As of January 1, 2022, more than 4 million females living in the U.S.A are known to have a case history of the invasive breast cancer [2]. Current treatment methods are chemotherapy, radiotherapy and surgery. Chemotherapy remains to be the most common method of treatment with some limitations [3]. Administered drug in chemotherapy is not targeted and effects healthy tissues and may accumulate in certain parts of the body.

Therefore, it is documented that chemotherapeutic agents can cause serious organ (kidney, lung, liver etc.) damage [4]. For this reason, arranging drug concentrations where antitumor effect can be achieved can also cause toxic effects on healthy cells. When chemotherapeutics are used in lower concentrations, the desired therapeutic level may not be achieved. These restrictions have created a need for drug delivery systems (DDS) based on nanotechnology that can improve bioavailability, biocompatibility and controlled release of drugs [5–7]. Among various vectors as DDSs, lipid-based nanocarriers are the most favorable candidates for drug delivery due to their physiologically-related nature [8]. NLCs are the new-generation lipid nanoparticles consisting of both solid and liquid lipids at room temperature which causes a defective crystalline structure and play a significant role in biomedical applications such as drug delivery, gene transfer, and imaging, utilizing the properties of soft matter [9,10]. This can provide more available regions for drug encapsulation, especially for hydrophobic drugs [11]. NLCs that contain liquid lipid nano-compartments in their structure are called multiple-type (Type-III) NLCs [12,13]. This type NLCs come into prominence to increase the drug loading capacity and provide a more controlled release because of the lower solubility of the drug in solid lipid than liquid lipid [12]. In this way, the drug dissolves more in the liquid lipid compartment, while the outer solid lipid matrix helps for prolonged release.

The utilization of photothermal therapy (PTT) alongside chemotherapy has significant benefits for cancer treatment [14–18]. During the PTT procedure, the use of photothermal agents leads to the conversion of light into heat. This heat generated is then used to destroy cancer cells through thermal ablation, causing their death [19]. The outstanding advantages of PTT include few side effects, low toxicity, non-invasive and localized properties, especially avoidance of chemo-resistance [20,21]. NIR light is the preferred choice for practical applications due to its low attenuation by soft tissues and blood, enabling it to penetrate tissues better than other wavelengths of light [19]. AuNPs are ideal agents for PTT due to their exceptional plasmonic characteristics and low toxicity. AuNPs can be deposited within tumors by active or passive targeting [22]. They can also be activated by a NIR laser irradiation, inducing irreversible cell damage by allowing sufficient heat generation at low laser powers, denaturing proteins, and breaking cell membranes directly within the tumor, minimizing side effects [23]. Among the golds with good photothermal conversion efficiency in the NIR-I region (650–980 nm), AuNSs, AuNRs and AuNCs can be given as examples [24,25]. The use of AuNPs in high concentrations accumulates in the main organs, especially in the kidneys [26]. For this reason, in such studies, it is necessary to pay attention to the concentration and even the size of the particles. On the other hand, high concentration and high surface area are very important to reach the desired temperature for hyperthermia [27,28]. In order to eliminate these negative effects, the encapsulation of inorganic nanoparticles into the carrier system has great importance [29]. AuNPs and drug can be loaded into DDSs simultaneously and their distribution in the body can be controlled. Moreover, the therapeutic success of PTT is strongly dependent on the cancer type, and the tumor adaptation to temperature [30]. Employing combined therapeutic methods that rely on the synergistic interaction between heat and cytotoxic treatments has been suggested as a highly advantageous approach [31]. Multiple studies have indicated that combining DNA damaging agents like DOX with hyperthermia is more effective as DNA repair processes are temperature-dependent [32]. DOX is an anthracycline compound that primarily inhibits the topoisomerase I and II and intercalate into DNA, thus inducing programmed cell death. Nevertheless, DOX has a significant toxic effect on healthy tissues which is a major problem that should be addressed while conceptualizing an efficient cancer treatment.

The presented study focuses on the development of drug-assisted chemo/photothermal agents to benefit from their synergistic cytotoxicity on triple negative breast cancer (TNBC) cells MDA-MB-231, on-demand and targeted release of DOX by using AuNSs, AuNRs and AuNCs individually as photothermal agents and by this way evaluating the effect of geometry on the photothermal efficacy of AuNPs under NIR irradiation (808 nm). Our findings show that, (DOX+AuNRs)@NLCs possessed the most cytotoxic effect under NIR irradiation whose inhibition on cell viability is higher than the total inhibition of DOX NLCs and AuNRs NLCs individually applied which proves the synergistic antitumor efficacy of the developed formulations. Finally, it has been demonstrated that lipid-based biocompatible nanoparticles that can provide a synergistic therapeutic effect can be successfully prepared by utilizing inorganic NPs with appropriate geometry and concentration, and lipid NPs with the correct composition and appropriate drugs.

2. Experimental methods

2.1. Materials

Pluronic F-127, gold (III) chloride trihydrate, sodium chloride, sodium phosphate monobasic monohydrate, sodium phosphate dibasic dodecahydrate, chloroform, and methanol were purchased from Sigma Aldrich (St. Louis, MO, USA). Stearic acid, oleylamine, tween-20 were purchased from Merck (Darmstadt, Germany). Oleic acid (OA) and sodium bicarbonate were obtained from Fisher Chemicals (Loughborough, UK). Tert-Butylammonium bromide was obtained from Acros Organics (Carlsbad, CA, USA). Doxorubicin hydrochloride was purchased from Toronto Research Chemicals (North York, Canada). Ultrapure water with a resistivity of 18.2 MΩ·cm was used for all experiments as a water purification system (Millipore Direct-Q3 UV). All materials were used without further purification.

2.2. Preparation of AuNPs with different geometry

Oleylamine-coated AuNSs were synthesized to be used as a photothermal agent. For the preparation of AuNSs, 5 mL of chloroform, 1 mL of oleylamine, and 0.05 g of $HAuCl_4 0.3\ H_2O$ were allowed to mix for 10 min at 30 °C at atmospheric conditions. Then, 0.04 g TBAB, 0.05 mL oleylamine, and 1 mL chloroform were mixed with sonication and added to the mixture at 30 °C. At this stage, the color was recorded as dark purple. The mixture was stirred for 45 min using a magnetic stirrer. Then, the samples were centrifuged three times with ethanol at 14,000 rpm to separate the uncoated oleylamine of the AuNSs surface. After centrifugation, the samples were left to dry in a vacuum desiccator for 24 h and stored in eppendorfs at + 4 °C.

AuNRs were synthesized using the seed-growth method by slightly modified El-Sayed and his co-workers procedure [33]. A total of 0.25 mL $HAuCl_4$ solution from 10 mM and 10 mL of a CTAB solution from 0.1 M were mixed at 30 °C. Then, $NaBH_4$ solution (0.60 mL of 10 mM) was quickly added into the previous solution under vigorous stirring without using a magnetic stirrer. At this stage, the $NaBH_4$ solution should be ice cold. The final seed solution was stirred for 5 min to ensure the decomposition of excess NaBH4. The silver(I)-assisted growth part was started by mixing of 0.5 mL $HAuCl_4$ (10 mM) and 0.1 mL $AgNO_3$ (10 mM) with 10 mL CTAB solution (0.1 M). Then, 0.2 mL HCl (1.0 M) was added to the solution, and the pH was reduced to 3–4. This step is to stabilize the structure, so that the seed solution does not turn into a

dumbbell shape. Then, 0.08 mL L-ascorbic acid (0.1 M) was added into the solution to reduce the gold from Au(III) to Au(I). In the final step, 24 μL of seed solution was added to the growth solution, and the solution was kept at 30 °C under gentle stirring for 2 h. AuNCs were synthesized using the seed-growth method by slightly modified Narayanan et al. procedure [34]. 0.25 mL of $HAuCl_4$ solution from 0.01 M and 7.5 mL of a CTAB solution from 0.1 M were mixed slightly at 30 °C. Then, $NaBH_4$ solution (0.60 mL of 10 mM) was quickly added to the previous solution under vigorous stirring without using a magnetic stirrer. At this stage, the $NaBH_4$ solution should be ice cold. The final seed solution was stirred for 2 min to ensure the decomposition of excess $NaBH_4$ and the seed solution was kept 2 h without stirring. The preparation of growth solution started by mixing of 0.2 mL $HAuCl_4$ (10 mM) and 0.3 mL $AgNO_3$ (10 mM) with 4.75 mL CTAB solution (0.1 M). Then, 0.032 mL L-ascorbic acid (1 M) was added to the solution to reduce the gold from Au(III) to Au(I). In the final step, 10 μL of seed solution was added to the growth solution, and the solution was kept at 30 °C without stirring for 3 h. To remove free CTAB molecules, the aqueous solution of AuNPs was centrifuged at 10,000 rpm for 30 min. After centrifugation, the supernatant which was rich in CTAB molecules was removed, and pure water was added to the solid part at the bottom. This process was repeated two times.

2.3. Preparation of (DOX+AuNPs)@NLC

In this study, NLC was prepared as a drug carrier particle by the melt-emulsification method as described in the literature [35]. Briefly, 95 mg mixture of stearic acid and oleic acid were mixed and added to the mixture of DI water (30 mL) and Pluronic F-127 (98.4 mg) when both solutions reached 75 °C. Oleic acid used as a liquid lipid was increased from 0% to 40%. Prior to addition to the water phase, acetone and ethanol were also added into the stearic acid-oleic acid mixture for easier emulsification. Then, this emulsion was left to freeze for 3 h at −20 °C without waiting in room temperature.

To prepare (DOX+AuNPs)@NLC, specific amounts DOX and AuNPs were added to the mixture of the oil phase consisting of oleic acid and stearic acid. Then, DOX and AuNPs loaded oil phase was integrated into the water phase, which contained DI water and surfactant, and the procedure was completed similarly as mentioned NLC preparation. While loading the active ingredient into the NLC, two different ratios were carried out, 1:15 and 1:144 (drug:lipid, (w/w%)).

2.4. Characterization of (DOX+AuNPs)@NLC

Hydrodynamic diameters of NLC, AuNSs, AuNRs, AuNCs, and (DOX+AuNPs)@NLC were determined by dynamic light scattering (DLS, ALV-CGS-3 Compact Goniometer) at a 90° angle by diluting the 1:100 ratio with DI water. Atomic Force Microscopy (AFM, PSIA Corporation, XE-100E)) was also used to examine the size and morphology of the NLCs. AFM samples were prepared by drying the samples under a vacuum for 24 h at room temperature. Also, Transmission Electron Microscopy (TEM) analysis was performed to get more detailed information about sizes and morphology.

2.5. Encapsulation efficiency (EE%) and drug loading capacity (DL%)

The NLC dispersion was centrifuged at 8000 rpm for 15 min to determine the amount of free DOX which was not encapsulated in NLC. The absorbance value of the supernatant was measured by UV–vis Spectrophotometer (UV–vis, Thermo Scientific™, GENESYS 10 S) at 485 nm. The encapsulation efficiency and drug loading were calculated using Eq. 1 and Eq. 2, respectively [36].

$$EE\% = \frac{Total\ \ amount\ \ of\ \ drug - Free\ \ amount\ \ of\ \ drug\ \ in\ \ the\ \ supernatant}{Total\ \ amount\ \ of\ \ drug} x100 \quad (1)$$

$$DL\% = \frac{Total\ \ amount\ \ of\ \ drug - Free\ \ amount\ \ of\ \ drug\ \ in\ \ the\ \ supernatant}{Total\ \ amount\ \ of\ \ drug + Total\ \ amount\ \ of\ \ lipid} x100 \quad (2)$$

2.6. In vitro DOX release and NIR triggered release

The release of DOX from NLCs was investigated separately in the presence of AuNSs and only in the presence of active pharmaceutical ingredients. Drug release experiments were carried out in 50 mL PBS solution, which contains 0.7% (w/v%) Tween-20 at 37 °C. 1 mL (0.32 mg drugs/mL) of drug-loaded NLC dispersion was placed in the membrane and added to the release medium considering the sink conditions. Experiments were also carried out at pH 7.4 and pH 5.5, respectively to mimic blood pH and cancer cell pH. Absorbance values were recorded at regular time intervals (0, 0.25, 0.50, 1, 2, 4, 6, 24, 30, and 48 h), and releases were observed for 48 h. All experiments were performed at least three times.

2.7. Photothermal performance studies

AuNSs NLC, AuNRs NLC, and AuNCs NLC dispersions were prepared at specific concentrations (7.8, 13, 26, 39, 52 μg Au/mg lipid) in a volume of 1.2 mL and poured into the quartz cuvette. The NIR laser source (CNI Model with PSU-III-LED, MDL-III-808–2.5 W) is positioned to coincide with the midpoint of the quartz cuvette. A heat chamber was used to maintain the ambient temperature. The temperature values were recorded every 10 s. NIR irradiation was applied at various power values (1–2.5 W) at 808 nm for 15 min. These laser experiments were repeated by increasing the NLC concentration and keeping the AuNSs, AuNRs and AuNCs amounts constant. A rotary evaporator was used to adjust the concentration of NLC. FLIR E54 model thermal camera was used to record the temperature increase. All experiments were repeated at least three times.

In addition, an on-off cycle study was carried out to test how long the particles could maintain their activity. After the particles were exposed to NIR irradiation, the laser source was turned off. Recooling at room temperature was recorded every 10 s, and on-off cycles were repeated three times. The photothermal conversion efficiencies of the particles were calculated from Eq. 3.

$$\eta = \frac{hS(T_{\max} - T_{surr}) - Q_{diss})}{I(1 - 10 - s^{\lambda})} \quad (3)$$

Here, h is the heat transfer coefficient, S is the surface area of the quartz bath, T_{max} is the maximum steady temperature of dispersion, and T_{surr} is the environmental temperature. Also, Q_{dis} refers to the heat emitted from the absorbed light with both the quartz cuvette cell and the dispersion, which is not included in AuNPs. I refer to the laser power and λ is the absorbance of the dispersion at a wavelength of 808 nm [37].

2.8. Cell culture studies

The TNBC, highly metastatic breast cancer cell line, MDA-MB-231, was purchased from the American Type Culture Collection (ATCC, Wesel, Germany). Cells were cultured in High Glucose DMEM (Capricorn, Germany) containing 10% fetal bovine serum (Capricorn, Germany), 1% L-glutamine (Sigma-Aldrich, Milan, Italy) and 1% Antibiotic solution (BIOIND, Israel). Culture conditions consist of 37 °C, 5% CO_2 and 100% humidity.

2.9. Cell metabolic activity analysis

Cytotoxicity studies were performed using the MTT assay. The of control, NLC, drug and different geometry of AuNPs, drug and different geometry of AuNPs containing NLCs, with or without NIR irradiation were applied to MDA-MB-231 cells cultured in 96 well plates. Analyses were carried out for ten experimental groups. The effects of different compounds on the metabolic acitivity of breast cancer cells were measured by spectrophotometer. Briefly, 5000 cells per well for each experimental group were seeded in 96-well plates (Nest Scientific USA Inc.) and incubated at 37∘C with 5% CO_2. 10 μL of MTT final concentration 0.5 mg/mL solution (Biotium,California, USA) was added to each well at 0, 24 and 48 h. Plates were incubated for 4 h in the dark at 37 °C. Then, 100 μL of DMSO was added to each well to dissolve the formazan crystals. It was mixed by pipetting and left for 15 min to ensure complete dissolution. Absorbance was recorded at 570 nm by a microplate reader (BioTek Synergy H1, BioTek Instruments, Winooski, VT, USA). The viability is expressed as control OD percent.

2.10. Lateral motility assay

In order to test the metastatic potential of highly metastatic MDA-MB-231 cells after treatment, the lateral motility was examined by performing the wound healing assay. The cells (2×10^5 cells per well) were seeded in six-well plates (Nest Scientific USA Inc.). After they reach confluency, three wounds were produced in each well using a pipette tip. The wells were rinsed once with fresh medium, and wound widths were recorded under an inverted microscope (Leica, Wetzlar, Germany). These cells were treated with NLC, DOX and DOX NLC for 48 h. Pictures of wound areas at 0, 24 and 48 h were measured with an NIH Image J program and adopted as 100 in the beginning and expressed as percent remaining cell free areas.

3. Results and discussion

3.1. Preparation and characterization of AuNPs

The primary objective of our study was to prepare AuNPs in appropriate sizes and desired geometries (sphere, cube and rod) and then encapsulate them with the preferred antitumor agent (DOX) into biocompatible NLCs with high encapsulation efficiency to use in chemo/photothermal synergetic therapy.

It is well-known that, according to both Mie's theory and experimental findings, AuNPs bigger than 20 nm which can be counted as a particle different than a bulk material, possess a spectrum which is composed of the sum of size-dependent absorption and scattering modes. Higher order modes become more dominant with increasing particle size, causing the plasmon absorption band to red shift and resulting in increased bandwidth. The optical absorption spectra depend directly on the size of the particles, which is called the extrinsic size effect. AuNSs are symmetrical particles and the plasmon resonance of this type of geometry collected on the same axis and band. However, the plasmon resonance for nanorods splits into two different bands. Moreover, as the aspect ratio increases, the energy separation between the resonance frequencies of the two plasmon bands increases [38]. The high energy band corresponds to the oscillation of the electrons perpendicular to the major axis of the rods and is referred to as the transverse plasmon absorption. The other absorption band, which is red-shifted to lower energies, is caused by the oscillation of the electrons along the major axis of the nanorods and is known as the longitudinal surface plasmon absorption [39]. In Fig. 1. A, Fig. 1. B and Fig. 1. C the UV-vis spectra of AuNSs, AuNRs, and AuNCs prepared in our study is

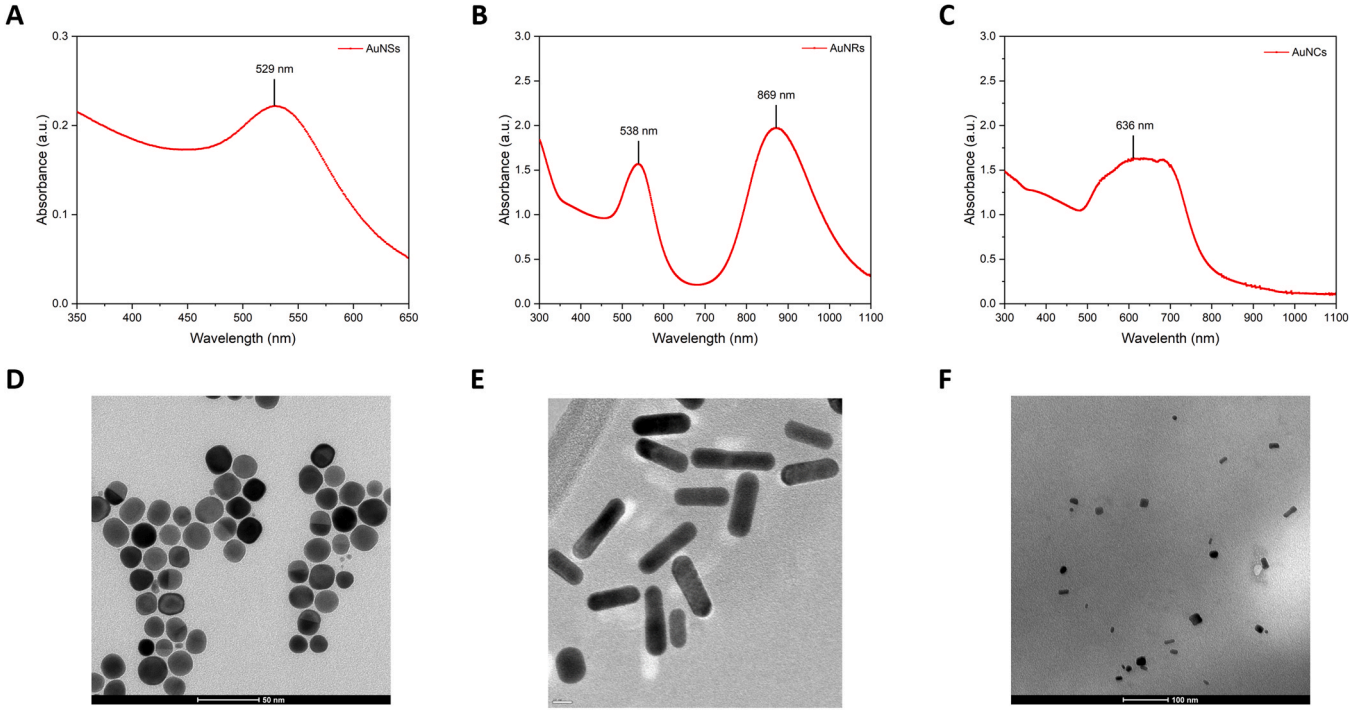


Fig. 1. UV–vis spectrum of A) AuNSs and B) AuNRs C) AuNCs and TEM images of D) AuNSs and E) AuNRs F) AuNCs (the bar is 50 nm for AuNSs and AuNCs, 100 nm for AuNRs).

presented, respectively. AuNSs exhibited a single peak value at 529 nm, as expected. It is known that AuNPs with spherical geometry do not give a surface plasmon resonance (SPR) peak in the NIR region and the characteristic absorbance band gap of AuNSs was seen between 500 and 600 nm in the visible region. On the other hand, in Fig. 1. B, it was determined that the AuNPs with rod geometry consist of two peaks at 538 and 869 nm. One of the two plasmon bands found in AuNRs is the "longitudinal LSPR band" (at 869 nm) interrelated with electron oscillations along the length axis. The other one is the "transverse LSPR band" (at 538 nm) excited by light polarized along the transverse direction of the AuNRs [39]. For the cubic particles, as given in the literature, when the particle geometry is a regular cube, a single plasmon band is seen, unlike the asymmetric AuNRs [40]. Although the AuNCs used in our study are not in a perfectly regular cube structure (Fig. 1. C), they formed a single plasmon band at 636 nm, since they have a shape similar to the geometry of a faceted rectangular prism whose side lengths are close to each other.

In addition, the sizes and geometries of these particles were analyzed by TEM. The average diameter of the AuNSs was calculated as 18.6 ± 3.21 nm (Fig. 1. D). This size value was suitable for loading AuNPs into NLC. In order to make this process easier, the surface of the AuNPs was coated with oleylamine and the hydrophobicity was increased. On the other hand, in Fig. 1.E., the longitudinal length of the AuNRs was calculated as 59.5 ± 28.94 nm and the width as 10.2 ± 3.34 nm. Aspect ratio was also calculated as a 5.85. In Fig. 1.F., the edge length of the cubes was recorded as 23.7 ± 17.34 nm.

3.2. Preparation and characterization of (DOX+AuNPs)@NLC

NLC was prepared by using the "melt-emulsification method" with changing many parameters such as mixing time, type of emulsifier, amount of surfactant, mixing way and mixing speed. The size of NLCs, which were prepared in 10 different formulations are presented in Table S1. In the melt-emulsification method, surfactants are added to the water phase. One of the main reasons for this is that during the solidification of the particles, the surfaces of the lipid droplets are rapidly coated with surfactants, thereby reducing the particle size. For this, Tween-20 and Pluronic F-127 were used as emulsifying agents, and in the case of using Pluronic F-127 (1%, (w/w%)), smaller diameter NLCs were obtained. In addition, when the mixing speed was increased, smaller NLCs were formed.

Similarly, the duration and type of mixing affect the size. For synergistic therapy, intravenous administration of drug carriers will be the preferred route. For that reason, it was preferred to have the NLC in the range of about 500 nm. Therefore, our primary motivation was to produce NLC with the as smallest as possible in size. Because, its expected that the size would increase when DOX and gold were loaded into the NLC which leads us to continue with NLC_8 which the smallest size, 66.35 ± 14.85 nm.

After the optimization studies of the NLCs were completed, DOX and AuNPs were added to the NLC to investigate size (Table 1). When DOX was added to the NLC at a ratio of 1:15 (drug:lipid), the NLC size was increased 66.35 ± 14.85 nm to 372.20 ± 70.47 nm. Also, the AuNSs and AuNCs were encapsulated to the NLC at a lipid ratio of 26 μg Au/mg lipid and their sizes are 290.12 ± 58.15 nm and 344.82 ± 54.23 nm, respectively. and AuNRs were encapsulated to the NLC at a lipid ratio of 19.5 μg Au/mg lipid and its size was calculated as 302.13 ± 62.98 nm. The size obtained when only DOX was loaded higher than when only AuNP was loaded. This is because a large amount of DOX can be dissolved in the incompatible oleic acid within the matrix of NLC. When DOX and each of the AuNP were loaded together, the size of NLCs increased between 317.92 ± 49.84 nm and 374.80 ± 67.93 nm. The reason for the increase in size is due to solid DOX and AuNPs occupying a large space in the NLC matrix. This size increase was one of the indications of the successful encapsulation of DOX and AuNPs into NLCs [29]. Looking at the literature, Zheng et al. added DOX and polyhedral AuNPs into NLC. Similar to this study, the NLC size of 267 nm increased to approximately 378 nm when both DOX and AuNPs were encapsulated. Besides in our study, the encapsulation efficiency of DOX NLC was 82.75%, increasing to approximately 90% when AuNPs were included (Fig. 2). Gold geometry did not significantly change the DOX encapsulation efficiency and loading capacity.

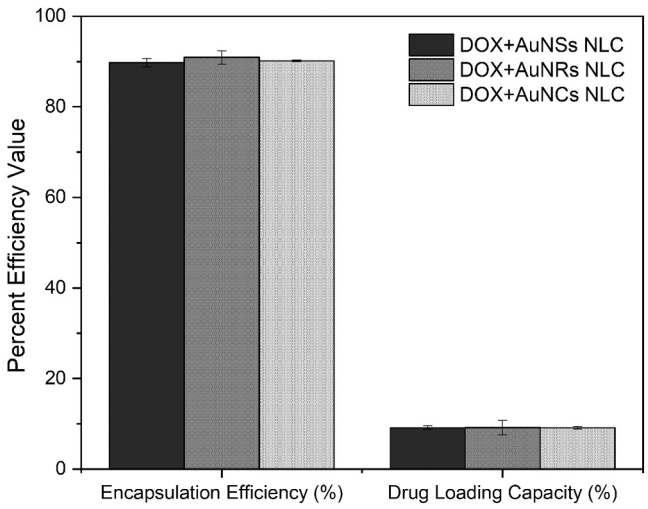


Fig. 2. Percent encapsulation efficiencies and drug loading capacities of DOX+AuNSs NLC, DOX+AuNRs NLC, DOX+AuNCs NLC.

3.3. Photothermal performance of AuNSs NLC, AuNRs NLC and AuNCs NLC

The particles were exposed to NIR light irradiation and temperature changes were observed. Fig. 3.A. shows the temperature change profiles of different concentrations of AuNSs loaded NLCs studying under 808 nm NIR irradiation at 2.3 W power for 15 min. The temperature of pure water increased by 0.7 °C. On the other hand, at 52 μg Au/mg lipid, the highest concentration studied, the temperature was increased to 53.3 °C from 21.1 °C. So, the temperature difference was calculated as 32.2 °C. Similarly, the temperature differences were noted as 9.8, 11.4,

Table 1
Sizes for NLC, DOX entrapped NLC, AuNPs entrapped NLC and AuNPs and DOX co-entrapped NLC.

		Size (nm)	
	PDI	**DLS**	**AFM**
NLC	0.124 ± 0.06	72.02 ± 24.87	66.35 ± 14.85
DOX NLC	0.170 ± 0.02	263.46 ± 38.15	372.20 ± 70.47
AuNSs NLC	0.232 ± 0.02	238.56 ± 24.16	290.12 ± 58.15
AuNRs NLC	0.507 ± 0.02	227.76 ± 81.78	302.13 ± 62.98
AuNCs NLC	0.527 ± 0.01	294.28 ± 92.01	344.82 ± 54.23
DOX+AuNSs NLC	0.422 ± 0.06	487.45 ± 62.80	352.13 ± 29.34
DOX+AuNRs NLC	0.514 ± 0.04	412.15 ± 71.15	317.92 ± 49.84
DOX+AuNCs NLC	0.502 ± 0.04	468.56 ± 81.64	374.80 ± 67.93

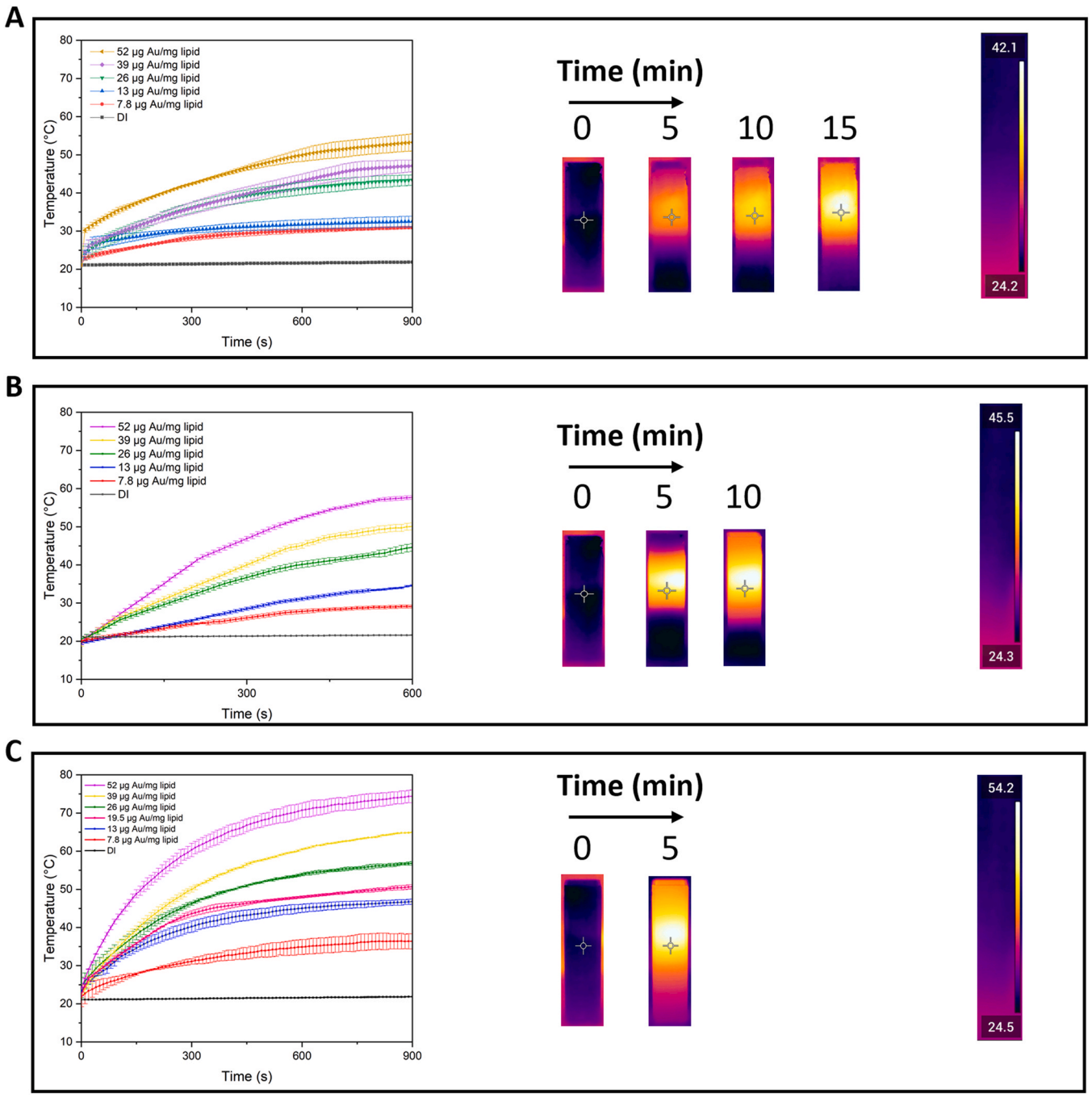


Fig. 3. Temperature change profiles and thermal camera images of NLC dispersions containing different concentrations of (7.8–52 µg Au/mg lipid) A) AuNSs, B) AuNCs, C) AuNRs at 808 nm NIR irradiation, 2.3 W power. [n = 3].

22.3, 26.0 and 22.3 °C for 7.8, 13, 26 and 39 µg Au/mg lipid, respectively. It can be deduced the AuNSs in the NLC increased and the temperature reached at the end of 15 min also increased. The appropriate temperature range for hyperthermia, 41–45 °C, was reached at a lipid concentration of 26 µg Au/mg lipid. For AuNSs NLC at this concentration, the temperature was recorded as 43.4 °C after 15 min. However, since temperatures exceeding 45 °C are disadvantageous for healthy cells, 26 µg Au/mg lipid was used as the optimum concentration value for further studies related to spherical geometry.

In Fig. 3. B, an experimental set similar to AuNS was created with AuNRs. When the samples were exposed to NIR laser radiation for 15 min, it was observed that this time moved away from the desired temperature value (41–44 °C). Only 5 min was suitable for these concentration and power values. So, at the end of 5 min, the temperature differences were also calculated as 9.3, 16.8, 20.9, 22.0, 27.5 and 36.4 °C for increasing concentrations, respectively. It was observed that the values obtained against the same concentrations with AuNSs were higher in rod-shaped gold. One of the reasons for this, the AuNRs have a larger surface area than AuNSs. The other reason is that the SPR band splits into two bands when the shape of the AuNRs changes from AuNSs. In addition, Sangnier et al., as a result of their study, proved that nanospheres are only suitable for the NIR-1 region and that at 808 nm, nanorods show more temperature increase than nanospheres. In this study, it was determined that AuNPs encapsulated in NLCs similar results. The optimum concentration value for AuNRs was 19.5 µg Au/mg lipid exposed to laser irradiation at 2.3 W for 5 min. At this

concentration, the temperature reached 43.6 °C degrees. As mentioned earlier, cell death can be induced at temperatures above 41 °C. However, cells are reported to undergo necrosis at a higher temperature of 46 °C or higher [41]. While selecting the optimal concentration, was kept of the range of apoptosis.

The set of experiments examining the photothermal effects of AuNS and AuNRs was also done with AuNCs. Fig. 3. C shows the variation of the temperature profiles of AuNCs loaded NLCs with increasing concentration. The temperature changes obtained for AuNCs were calculated as 9.1, 15.1, 24.0, 30.7 and 38.1 °C respectively, from 7.8 μg Au/mg lipid to 52 μg Au/mg lipid. Similar to gold in other geometry, it is seen that the temperature values reached increase as the AuNCs concentration in the NLC increases. Here, 26 μg Au/mg lipid was chosen as the optimum concentration. This concentration determination was made with attention to cell apoptosis. In order to understand the photothermal property differences between AuNPs, the external conditions were kept the same and the 26 μg Au/mg lipid concentration was used. For comparison, the heating provided by AuNPs in each geometry was recorded for 10 min. The temperatures of AuNRs NLC, AuNCs NLC and AuNSs NLCs increased to 53.9, 44.6 and 41.2 °C in these conditions, respectively. A temperature difference of 29.6 °C for AuNRs NLCs, 24.0 °C for AuNCs NLCs and 20.1 °C for AuNSs NLCs was recorded for 10 min under 808 nm NIR irradiation. Thus, the particles with the best performance in terms of the temperature difference they create were AuNRs NLC, AuNCs NLC and AuNSs NLC, respectively.

The thermal camera images of the AuNPs with three different geometries were brought together. Here, it is clearly seen that the AuNRs NLC can reach the desired temperature with less concentration in a shorter time. It is a crucial subject since inorganic particles like AuNPs can cause accumulation in the human body if given in high concentrations. Moreover, the longer the exposure in the cancerous area with NIR irradiation, the higher the chance of necrosis in the cells. For this reason, it is proven that the AuNRs are much better photothermal agents than their other geometrical counterparts considering their superior performance with lower concentrations in a shorter time during the NIR treatment.

The amount of AuNPs in the NLC dispersion was kept constant, whereas the amount of NLCs loaded with AuNPs was doubled in the same volume and is equivalent to the 52 μg Au/mg lipid concentration (Fig. S1). While heating with laser, by doubling the concentration, AuNSs (Fig. S1. A), AuNRs (Fig. S1. B), and AuNCs (Fig. S1. C), reached 54.4 °C at the end of 15 min, 61.43 °C at the end of 5 min, and 56.1 °C at the end of 10 min, respectively. These values were quite similar to the 52 μg Au/mg lipid concentration mentioned for 53.3 °C, 60.3 °C and 57.7 °C for AuNSs, AuNRs, and AuNCs, respectively. These results showed that at the same power value and laser wavelength, the photothermal properties always depend on the gold concentration, even though the number of NLC particles encapsulated with AuNPs was increased.

NLCs were exposed to NIR laser irradiation and the particles were allowed to cool until they reached a value close to the initial temperature in order to understand how stable the particles were and how long they could maintain their activity without any external effect. As a result of this study, AuNSs and AuNCs were stable until the third cycle (Fig. S2. A. and Fig. S2.C.). On the other hand, AuNRs are stable until the second cycle (Fig. S2. B). After these cycles, more temperature increase was measured in the same time period (data was not graphed). The better heating performance of AuNRs is significant in terms of reaching high temperatures in a shorter time and melting NLC. At this stage, it is thought that the gold-containing NLC particles cannot remain stable and diffuse from the NLC to the outer environment with disruption of NLC. Since AuNRs can convert more light into heat energy under the same conditions as AuNSs and AuNCs, so they can provide more heating in the desired area. Thus, AuNRs are presented as a successful photothermal agent in a short time and at lower concentrations compared to other studies.

The photothermal conversion efficiency values are given in Fig. S3. Here, time versus -ln(Q) graphs were drawn to obtain photothermal conversion efficiency values for all AuNPs (Fig. S3. A, Fig. S3. C and Fig. S3. E). From the graph drawn using the cooling curves of AuNPs, it was calculated that AuNSs (Fig. S3. B) had 18.17%, AuNRs (Fig. S3. D) 30.49%, and AuNCs (Fig. S3. F) 11.89% photothermal conversion efficiency, respectively. This disparity in efficiency for the three different geometry AuNPs is believed to be due to differences in the absorption coefficient associated with the absorption cross-section, which determines the ability of the plasmonic nanostructure to absorb light at a given level. Photothermal conversion efficiency values seem low, the fact that the gold was encapsulated in the NLC has reduced their efficiency percentages. While the conversion efficiency of AuNRs alone was 60.4%, this efficiency was almost halved when entrapped into NLC. Another reason for the variation in the efficiency was the concentration. In our study, we tried to keep the concentrations low to reduce toxicity taking into account the accumulation in healthy tissue. Here, we tried to emphasize the importance of loading AuNPs into NLC by considering many parameters such as irradiation time and concentration while keeping the photothermal conversion efficiency higher.

When only the release of DOX at pH 7.4 was examined, it reached approximately 36% at the end of 48 h (see Fig. 4. A). On the other hand, released DOX amount decreased to 20.3% when it is co-encapsulated with AuNSs at the end of first 7 h in Fig. 4.B. However, when NIR was applied to the particles for 15 min, the percent release was calculated as 48.5%. When only DOX was used, it was released into the environment at a concentration of 0.0010 mg/mL, while this value increased to 0.0014 mg/mL with the effect of NIR irradiation.

A similar release experiment was also performed for AuNRs as presented in Fig. 4.C. DOX release decreased to 22.4% when co-encapsulation with AuNRs. The decrease in percent release while increasing the encapsulation efficiency supports the better dissolution of DOX in the lipid matrix and its positioning towards the center of NLCs. When NIR irradiation was applied to the same structure for 5 min for 5 times, DOX release gradually increased to 54.7%. In addition, at the end of 5 times NIR applications, the released DOX concentration was calculated as 0.0015 mg/mL. At this point, the concentration is 2.4 times higher than that the case of NIR laser irradiation absences. In AuNCs NLCs, the percent release value, which was 26.6% without applying NIR, increased to 51.2% after applying NIR irradiation (see Fig. 4. D). In the presence of AuNCs, DOX concentration reached 0.0014 mg/mL at the end of release, similar to AuNSs. It was seen that AuNRs give proportionally better release performance with NIR irradiation**.** It was expected that AuNRs, which give the most successful results in photothermal properties, will be successful in NIR-triggered release. In triggering AuNRs with NIR irradiation, higher concentrations were achieved than other geometries. Because the temperature rise is also high in the steps where NIR irradiation was applied. The release, which started at 37 °C, increased its temperature by 0.19% at the end of the 5th cycle. After the first 2 steps, the temperature increase occurred in parallel with the on-off cycle experiments (see Fig. 4). The percentage concentration released in each NIR step was almost equal. On the other hand, NLC particles containing AuNSs and AuNC increased the release ambient temperature by 2.9 °C maximum and reached 39.9 °C degrees. DOX release from AuNSs and AuNCs NLCs was also calculated at similar concentration values at each step similar to AuNRs. Giu et al. used DOX and gold cluster-loaded liposomes in their studies [42]. They applied a NIR laser during the first 250 s to examine the DOX release change from the liposome. They recorded the temperature reached at the end of this period as 41.8 °C, similar to our study. They emphasized that this temperature value caused structural damage in the liposome. Similar to this proposition, AuNRs spread as a result of the disruption of NLCs at these temperatures may have increased the temperature gradually.

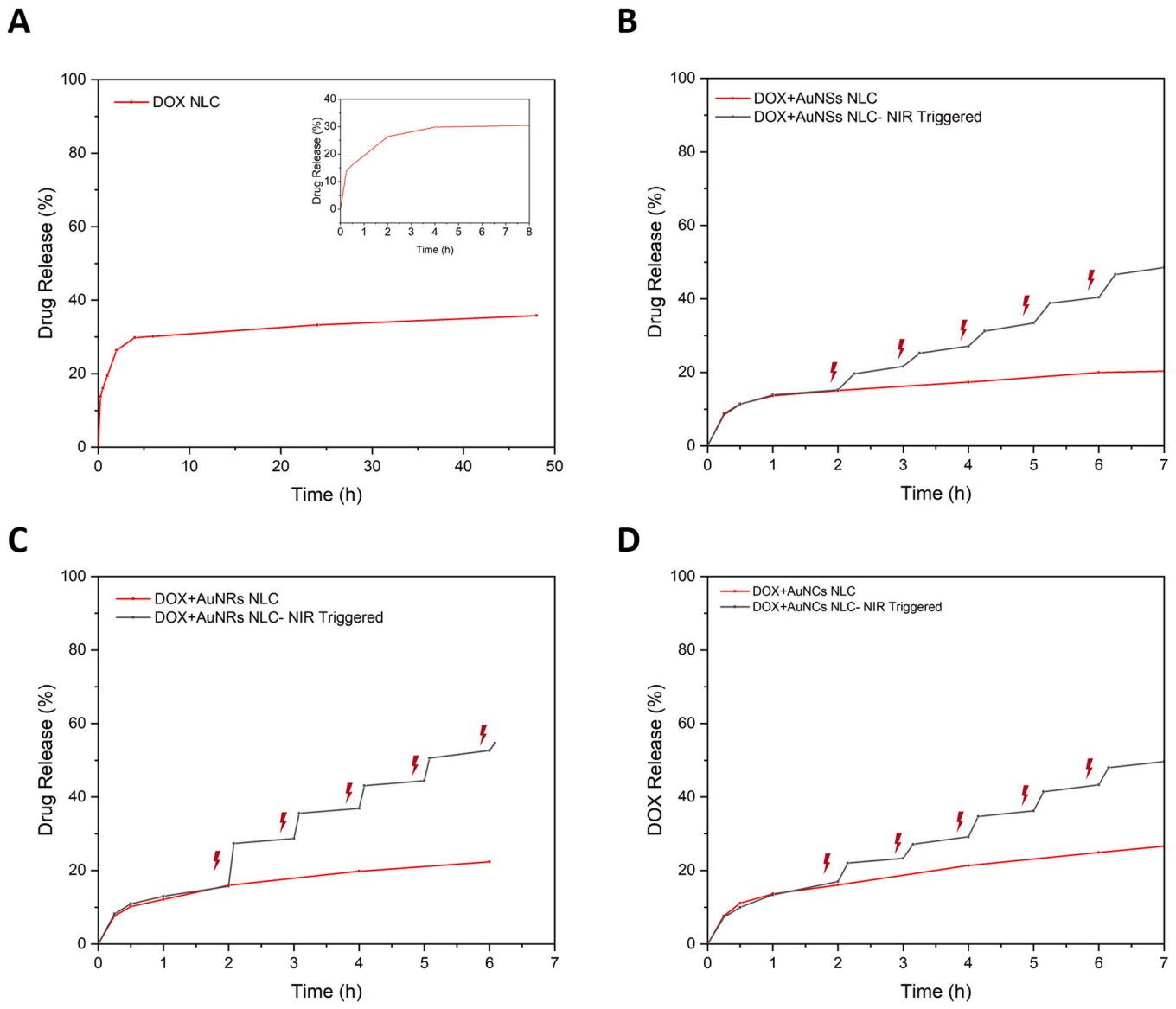


Fig. 4. In vitro release profile of A) DOX NLC, B) (DOX+AuNSs)@NLC with and without NIR irradiation (808 nm, 2.5 W, 15 min) C) (DOX+AuNRs)@NLC with and without NIR irradiation (808 nm, 2.3 W, 5 min) D) (DOX+AuNCs)@NLC with and without NIR irradiation (808 nm, 2.5 W, 10 min) at 7.4 pH in PBS solution (including 0.7% Tween-20 (w/v%)) at 37 °C.

3.4. . Cell studies

Motility is an essential feature of live cells. Cell migration is involved in the conception of life, embryonic development, immune response, and many pathological processes such as cancer metastasis and inflammation. The study of cell migration in cancer research is of particular interest as the main cause of death in cancer patients is related to metastatic progression. In our study, to get a prior information either NLCs had any adverse effect on lateral motility of MDA-MB-231 cells or a possible decrease on the anti-migration and antiproliferative effect due to encapsulation of DOX into NLCs, cell culture wound closure assay was applied. Lateral motility is expressed as % cell free area that remains and given in Fig. 5. It is observed that, application of NLCs alone, DOX-OA and NLC-DOX-OA resulted in 79%, 107%, 123% respectively while control cells closed the area by 71%. Therefore, NLC alone did not affect the lateral motility of cells but DOX loaded and DOX and OA containing NLC preparations caused a significant inhibition on lateral motility and therefore metastatic potential of cells. Also, the graphic represents the remaining cell free areas as percent of original wound in Fig. S4.

Cytotoxicity assays of free DOX, NLCs, DOX NLCs, AuNPs NLCs and (DOX+AuNPs)@NLCs were performed in human TNBC cell line MDA-MB-231 cells using the same concentration of in vitro studies for 24 h and 48 h (Fig. 6). In order to examine the effect of AuNP-induced localized hyperthermia on the cell proliferation in terms of both accelerated drug release and temperature-dependent DNA-damaging, NIR laser irradiation was applied at 808 nm. Except (DOX+AuNCs)@NLCs, (DOX+AuNRs)@NLCs, AuNCs NLCs and AuNRs NLCs; all the groups were equally treated with NIR for 15 min. In order to see the results of a realistic photothermal therapy application and to ensure that the local temperature does not exceed 42–43 °C, formulations containing AuNRs and AuNCs were irradiated just for 5 and 10 min, respectively. It is seen from the results given in Fig. 6, NLCs showed a negligible cytotoxicity on MDA-MB-cells with ~7% decrease in their percentage cell viability regardless with the application of laser. For DOX and DOX NLC, a reduction in the cell viability with 40.5% and 41.7% is observed, respectively, for the first 24 h. These differences increased to 52.1% and 65.4% for 48 h, with a larger gap, which can be accepted as a proof of the increase on the therapeutic effect of DOX with sustained release from

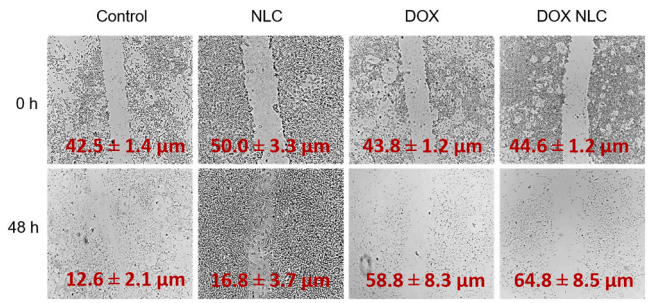


Fig. 5. Effects of NLC, DOX and DOX NLC on lateral mobility of MDA-MB-231 cells. Cells were treated NLC, DOX and DOX NLC in the micrographs of wound areas and the values represent the lateral distance.

NLCs. Moreover, to see the cytotoxic effect of AuNPs with different geometries on MDA-MB-231 cells, AuNPs NLCs were also used without DOX. For 48 h in the absence of laser irradiation, it was observed that AuNSs NLC, AuNCs NLC and AuNRs NLCs can reduce cell viability percentage to ~99.6%, ~101.3%, and ~102.3%, from ~128.0%, respectively. These results showed that AuNPs regardless with the geometry, have their own cytotoxicity on breast cancer cells. A number of in vitro studies have shown that AuNPs cores are nontoxic. However, there is a distinction between the AuNPs core and that of coating stabilizer, which is not possible to study the AuNPs core without a stabilizer. It is known that some precursors of AuNPs may be toxic, such as CTAB that is used in our study. However, in our study, the excess CTAB was successfully washed out via centrifugation, and accepted had no detectable effect on the cytotoxicity profile. Many reports in literature have shown that AuNPs exert their cytotoxicity through the induction of oxidative stress in various tumors [43]. It is also widely accepted that geometric properties can significantly alter the interaction of AuNPs with cells, cellular membranes and effect their intracellular localization and biodistribution. In their study, Steckiewicz and coworkers studied on the cytotoxicity of spherical, rod and star-shaped AuNPs on human fetal osteoblast hFOB 1.19 and pancreatic duct cell hTERT-HPNE cell lines and showed that rod-shaped AuNPs were the most toxic to human cells, while AuNPs spheres appeared to be the safest. In another study, it is reported that AuNRs were highly toxic in comparison to hexapod-shaped AuNPs. It is known that, according to the different geometries, the distribution of the surface atoms in AuNPs may have changed according to the different crystal properties of different parts. More atoms at angles and edges may cause stronger interactions with biomolecules. Thus, the higher toxicity of the rods and stars can be attributed featuring a larger number of edges and corners, which is often not observed for spherical AuNPs [44]. On the other hand, besides the geometry, there are two important parameters that can determine the extent of cytotoxicity of AuNPs which are size and concentration. As a general assessment, particles in the range of ~25–50 nm diameter have been found to exhibit the highest cellular uptake, whereas particles bigger than 50 nm show lower levels of uptake [45]. However, when the obtained results are evaluated in terms of Au concentration, it can be concluded that the Au concentration added to each well in cell studies is critical to explain the cytotoxicity behavior with a realistic approach. In their study, Wozniak and coworkers showed that, both for HEK293T cell line and HeLa cell line, when the concentration of AuNS, AuNR, Au nanoprisms and Au nanostars increased, the level of toxic behaviour increased which is seen at most for AuNSs [46]. However, it is also demonstrated that, 1 µM Au concentration exhibited a cytotoxicity which is statistically insignificant regardless of the particle geometry. The fact that the AuNP concentration was 0.4 µM/well in our study can be shown as one of the reasons of no significant toxicity occurred. Moreover, encapsulating AuNPs into the NLCs also has a vital role on that high biocompatibility. For the formulations without AuNPs, when the results with and without laser irradiation are compared, it can be said that NIR application does not make any difference when evaluated with respect to their own control groups. The decrease in the cell viability of NLC, DOX and DOX NLC after 24 h without laser application was observed as ~6%, ~36% and ~39% whereas under NIR irradiation the values became ~9%, ~40% and ~42%, respectively. The results exhibited that, without AuNPs, the toxicity of the formulations did not influence from the laser irradiation.

The significance of the synergistic approach is clearly seen when the cytotoxicity results of (DOX+AuNPs)@NLCs are examined to understand the effect of combined therapy in which photothermal therapy is used together with chemotherapy. In Fig. 6, it is seen that for both 24 h and 48 h, introduction of AuNPs besides DOX under NIR irradiation caused the most impactful cytotoxicity. When compared with DOX alone or DOX+NIR irradiation; (DOX+AuNSs)@NLC, (DOX+AuNCs)@NLCs and (DOX+AuNRs)@NLCs formulations caused much higher cell killing efficiency with ~49.2%, ~49.5% and ~47% decrement in the percent cell viability at 48 h. However, it should be underlined that in our study, according to the results given in Fig. 3; the formulations include AuNSs were exposed to 15 min, AuNCs 10 min, and AuNRs 5 min of NIR irradiation during cell studies. Although period of the applied NIR exposure differs, the fact that the obtained cell viability values are very close to each other means two things; i) AuNPs with different geometries show different photothermal potential under laser as mentioned before, and

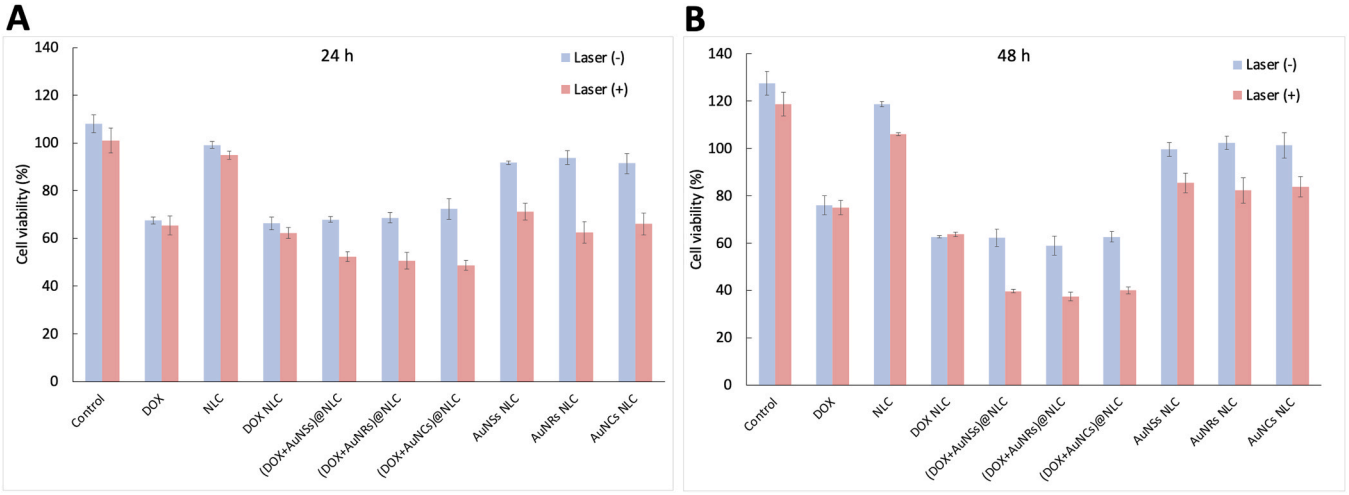


Fig. 6. Percentage of cell viability of control, NLC, drug and different geometry of gold nanoparticles, and drug and different geometry of gold nanoparticle containing NLCs at the end of A) 24 and B) 48 h, with or without NIR irradiation. Data represents mean three independent experiments (mean ± SD). n = 3.

ii) In addition to DOX-induced cell death, the effect of PTT-induced death is also significant. It is known that, PTT-induced local hyperthermia can permeabilize the interstitial matrices of tumors by denaturating the dense collagen matrix within the interstitial space between tumor cells and blood vessels [47]. In addition to that, PTT has been demonstrated to synergistically enhance the effectiveness of chemotherapeutic agents, particularly DNA-damaging agents like DOX which act as topoisomerase I and II inhibitors and DNA intercalating agents [48]. When the results given in Fig. 6. A and 6. B are examined, it is seen that under NIR irradiation, AuNPs NLC formulations were also able to create a significant toxicity especially for 24 h. For instance, the difference between the percentage cell viability values of (DOX+AuNRs)@NLC and AuNRs NLC is ~12%. However, it is also clearly seen that the same cytotoxic effect created by the heat shock was faded at the end of 48 h and the same difference increased to ~35%. These findings clearly shows that the cell killing efficiency obtained is not only due to local hyperthermia, but also to the synergistic approach of the combined use of DOX and AuNPs and the prolonged release of DOX from NLCs.

4. Conclusion

In conclusion, this study offers a dual chemotherapy/photothermal therapy approach using state-of-art (DOX+AuNPs)@NLC. In this study, gold nanoparticles in different geometries were used and after loading into the NLC, its potential for use in PTT was examined. AuNRs in NLC have been shown to be a good photothermal agent at 808 nm NIR irradiation. The drug loading capacity of (DOX+AuNRs)@NLC, which is approximately 304 nm in size, was calculated as 9.12%. Although NLCs have a higher drug loading capacity compared to their pure solid alternatives due to having low crystallinity, their encapsulation efficiency of highly water-soluble drugs such as DOX is comparably low. In further studies, conducting the experiments aimed at reducing the water solubility of DOX to increase its loading capacity can increase the drug encapsulation efficiency and thus therapeutic efficacy of the final nanocarrier. The structure being smaller than 500 nm indicates that it is suitable for intravenous use. In addition, in vitro cell studies have emphasized the significant impact of the use of photothermal therapy together with chemotherapy on cell viability. Furthermore, AuNRs are more successful photothermal agents than AuNSs and AuNCs in triggering NLC release. Thus, a biocompatible lipid-based carrier system suitable for synergetic therapy, which can be successful even in a system that is difficult to target, was presented. Also, a trojan-like smart lipid-based drug delivery system in which both AuNPs and DOX are encapsulated is presented.

CRediT authorship contribution statement

CE Okuyucu: Investigation, Visualization, Formal analysis, Methodology, Writing – original draft, Writing – review & editing. **GD Kalaycioglu:** Investigation, Visualization, Formal analysis, Methodology, Supervision, Writing – original draft, Writing – review & editing. **D Kacaroglu:** Investigation, Formal analysis. **AK Ozden:** Investigation, Formal analysis, Methodology, Writing – original draft. **N Aydogan:** Conceptualization, Supervision, Methodology, Recourses, Funding acquisition, Writing – original draft, Writing – review & editing.

Declaration of Competing Interest

The authors declare that they have no known competing financial interests or personal relationships that could have appeared to influence the work reported in this paper.

Data Availability

Data will be made available on request.

Acknowledgement

Authors acknowledge the financial support from Turkish Scientific and Research Council (TUBITAK) through the project 119M377.

Appendix A. Supporting information

Supplementary data associated with this article can be found in the online version at doi:10.1016/j.colsurfa.2023.131763.

References

[1] R. Siegel, K. Miller, H. Fuchs, A. Jemal, Erratum to "Cancer statistics, 2021", CA Cancer J Clin, 71 (2021) 7–33.
[2] K.D. Miller, L. Nogueira, T. Devasia, A.B. Mariotto, K.R. Yabroff, A. Jemal, J. Kramer, R.L. Siegel, Cancer treatment and survivorship statistics, 2022, CA: a cancer journal for clinicians, 72 (2022) 409–436.
[3] K.D. Miller, L. Nogueira, A.B. Mariotto, J.H. Rowland, K.R. Yabroff, C.M. Alfano, A. Jemal, J.L. Kramer, R.L. Siegel, Cancer treatment and survivorship statistics, CA: Cancer J. Clin. 69 (2019) 363–385.
[4] M.A. Perazella, Onco-nephrology: renal toxicities of chemotherapeutic agents, Clin. J. Am. Soc. Nephrol. 7 (2012) 1713–1721.
[5] S. Adepu, S. Ramakrishna, Controlled drug delivery systems: current status and future directions, Molecules 26 (2021) 5905.
[6] M. Naghdi, M. Ghovvati, N. Rabiee, S. Ahmadi, N. Abbariki, S. Sojdeh, A. Ojaghi, M. Bagherzadeh, O. Akhavan, E. Sharifi, Magnetic nanostructures in nanomedicine revolution: a review of growing magnetic nanocomposites in biomedical applications, Adv. Colloid Interface Sci. (2022), 102771.
[7] N. Jalilinejad, M. Rabiee, N. Baheiraei, R. Ghahremanzadeh, R. Salarian, N. Rabiee, O. Akhavan, P. Zarrintaj, A. Hejna, M.R. Saeb, Electrically conductive carbon-based (bio)-nanomaterials for cardiac tissue engineering, Bioeng. Transl. Med. 8 (2023), e10347.
[8] S. Samimi, N. Maghsoudnia, R.B. Eftekhari, F. Dorkoosh, Lipid-based nanoparticles for drug delivery systems, Charact. Biol. Nanomater. Drug Deliv. (2019) 47–76.
[9] M. Haider, S.M. Abdin, L. Kamal, G. Orive, Nanostructured lipid carriers for delivery of chemotherapeutics: A review, Pharmaceutics 12 (2020) 288.
[10] I. Chauhan, M. Yasir, M. Verma, A.P. Singh, Nanostructured lipid carriers: A groundbreaking approach for transdermal drug delivery, Adv. Pharm. Bull. 10 (2020) 150.
[11] B. Subramaniam, Z.H. Siddik, N.H. Nagoor, Optimization of nanostructured lipid carriers: Understanding the types, designs, and parameters in the process of formulations, J. Nanopart. Res. 22 (2020) 1–29.
[12] S. Wissing, R. Müller, The influence of the crystallinity of lipid nanoparticles on their occlusive properties, Int. J. Pharm. 242 (2002) 377–379.
[13] V.R. Salvi, P. Pawar, Nanostructured lipid carriers (NLC) system: a novel drug targeting carrier, J. Drug Deliv. Sci. Technol. 51 (2019) 255–267.
[14] M. Xie, N. Yang, J. Cheng, M. Yang, T. Deng, Y. Li, C. Feng, Layered MoS2 nanosheets modified by biomimetic phospholipids: enhanced stability and its synergistic treatment of cancer with chemo-photothermal therapy, Colloids Surf. B: Biointerfaces 187 (2020), 110631.
[15] Z. Jin, K.T. Nguyen, G. Go, B. Kang, H.-K. Min, S.-J. Kim, Y. Kim, H. Li, C.-S. Kim, S. Lee, Multifunctional nanorobot system for active therapeutic delivery and synergistic chemo-photothermal therapy, Nano Lett. 19 (2019) 8550–8564.
[16] J. Nam, S. Son, L.J. Ochyl, R. Kuai, A. Schwendeman, J.J. Moon, Chemo-photothermal therapy combination elicits anti-tumor immunity against advanced metastatic cancer, Nat. Commun. 9 (2018) 1074.
[17] M. Khafaji, M. Zamani, M. Golizadeh, O. Bavi, Inorganic nanomaterials for chemo/photothermal therapy: a promising horizon on effective cancer treatment, Biophys. Rev. 11 (2019) 335–352.
[18] B. Nasseri, E. Alizadeh, F. Bani, S. Davaran, A. Akbarzadeh, N. Rabiee, A. Bahadori, M. Ziaei, M. Bagherzadeh, M.R. Saeb, Nanomaterials for photothermal and photodynamic cancer therapy, Appl. Phys. Rev. 9 (2022), 011317.
[19] H.S. Han, K.Y. Choi, Advances in nanomaterial-mediated photothermal cancer therapies: toward clinical applications, Biomedicines 9 (2021) 305.
[20] J. Chen, C. Ning, Z. Zhou, P. Yu, Y. Zhu, G. Tan, C. Mao, Nanomaterials as photothermal therapeutic agents, Prog. Mater. Sci. 99 (2019) 1–26.
[21] V. Patel, C. Rajani, V. Tambe, D. Kalyane, N. Anup, P.K. Deb, K. Kalia, R.K. Tekade, Nanomaterials assisted chemo-photothermal therapy for combating cancer drug resistance, J. Drug Deliv. Sci. Technol. (2022), 103164.
[22] B.L. Jones, S. Krishnan, S.H. Cho, Estimation of microscopic dose enhancement factor around gold nanoparticles by Monte Carlo calculations, Med. Phys. 37 (2010) 3809–3816.
[23] L. Liu, X. Pan, S. Liu, Y. Hu, D. Ma, Near-infrared light-triggered nitric oxide release combined with low-temperature photothermal therapy for synergetic antibacterial and antifungal, Smart Mater. Med. 2 (2021) 302–313.
[24] B. Guo, Z. Sheng, D. Hu, X. Lin, S. Xu, C. Liu, H. Zheng, B. Liu, Biocompatible conjugated polymer nanoparticles for highly efficient photoacoustic imaging of orthotopic brain tumors in the second near-infrared window, Mater. Horiz. 4 (2017) 1151–1156.
[25] Y. Shi, J. Zhang, H. Huang, C. Cao, J. Yin, W. Xu, W. Wang, X. Song, Y. Zhang, X. Dong, Fe-doped Polyoxometalate as acid-aggregated Nanoplatform for NIR-II

Photothermal-enhanced chemodynamic therapy, Adv. Healthc. Mater. 9 (2020) 2000005.
[26] K.E. Ibrahim, M.G. Al-Mutary, A.O. Bakhiet, H.A. Khan, Histopathology of the liver, kidney, and spleen of mice exposed to gold nanoparticles, Molecules 23 (2018) 1848.
[27] X. Huang, M.A. El-Sayed, Gold nanoparticles: Optical properties and implementations in cancer diagnosis and photothermal therapy, J. Adv. Res. 1 (2010) 13–28.
[28] X. Huang, P.K. Jain, I.H. El-Sayed, M.A. El-Sayed, Plasmonic photothermal therapy (PPTT) using gold nanoparticles, Lasers Med. Sci. 23 (2008) 217–228.
[29] S. Zheng, S.Y. Song, J. Han, J.-O. Park, Combined photothermal-chemotherapy of breast cancer by near infrared light responsive hyaluronic acid-decorated nanostructured lipid carriers, Nanotechnology 28 (2017), 435102.
[30] B.C. Hancock, M. Parks, What is the true solubility advantage for amorphous pharmaceuticals? Pharm. Res. 17 (2000) 397–404.
[31] R. Li, X. Hu, F. Shang, W. Wu, H. Zhang, Y. Wang, J. Pan, S. Shi, C. Dong, Treatment of triple negative breast cancer by near infrared light triggered mild-temperature photothermal therapy combined with oxygen-independent cytotoxic free radicals, Acta Biomater. 148 (2022) 218–229.
[32] L. Pan, J. Liu, J. Shi, Nuclear-targeting gold nanorods for extremely low NIR activated photothermal therapy, ACS Appl. Mater. Interfaces 9 (2017) 15952–15961.
[33] M. Liu, P. Guyot-Sionnest, Mechanism of silver (I)-assisted growth of gold nanorods and bipyramids, J. Phys. Chem. B 109 (2005) 22192–22200.
[34] R. Narayanan, R.J. Lipert, M.D. Porter, Cetyltrimethylammonium bromide-modified spherical and cube-like gold nanoparticles as extrinsic Raman labels in surface-enhanced Raman spectroscopy based heterogeneous immunoassays, Anal. Chem. 80 (2008) 2265–2271.
[35] S. Mekhilef, R. Saidur, M. Kamalisarvestani, Effect of dust, humidity and air velocity on efficiency of photovoltaic cells, Renew. Sustain. Energy Rev. 16 (2012) 2920–2925.
[36] M. Joshi, S. Pathak, S. Sharma, V. Patravale, Design and in vivo pharmacodynamic evaluation of nanostructured lipid carriers for parenteral delivery of artemether: nanoject, Int. J. Pharm. 364 (2008) 119–126.
[37] X. Liu, B. Li, F. Fu, K. Xu, R. Zou, Q. Wang, B. Zhang, Z. Chen, J. Hu, Facile synthesis of biocompatible cysteine-coated CuS nanoparticles with high photothermal conversion efficiency for cancer therapy, Dalton Trans. 43 (2014) 11709–11715.
[38] D.P. Yang, D.X. Cui, Advances and prospects of gold nanorods, Chem. Asian J. 3 (2008) 2010–2022.
[39] S.M. Mousavi, S.A. Hashemi, S. Mazraedoost, K. Yousefi, A. Gholami, G. Behbudi, S. Ramakrishna, N. Omidifar, A. Alizadeh, W.-H. Chiang, Multifunctional gold nanorod for therapeutic applications and pharmaceutical delivery considering cellular metabolic responses, oxidative stress and cellular longevity, Nanomaterials, 11 (2021) 1868.
[40] D. Lee, S. Yoon, Gold nanocube–nanosphere dimers: preparation, plasmon coupling, and surface-enhanced Raman scattering, J. Phys. Chem. C 119 (2015) 7873–7882.
[41] M.R. Ali, Y. Wu, M.A. El-Sayed, Gold-nanoparticle-assisted plasmonic photothermal therapy advances toward clinical application, J. Phys. Chem. C. 123 (2019) 15375–15393.
[42] R. Gui, A. Wan, X. Liu, H. Jin, Retracted Article: Intracellular fluorescent thermometry and photothermal-triggered drug release developed from gold nanoclusters and doxorubicin dual-loaded liposomes, Chem. Commun. 50 (2014) 1546–1548.
[43] S.K. Surapaneni, S. Bashir, K. Tikoo, Gold nanoparticles-induced cytotoxicity in triple negative breast cancer involves different epigenetic alterations depending upon the surface charge, Sci. Rep. 8 (2018) 12295.
[44] P.M. Favi, M. Gao, L. Johana Sepúlveda Arango, S.P. Ospina, M. Morales, J. J. Pavon, T.J. Webster, Shape and surface effects on the cytotoxicity of nanoparticles: Gold nanospheres versus gold nanostars, J. Biomed. Mater. Res. Part A 103 (2015) 3449–3462.
[45] C. Carnovale, G. Bryant, R. Shukla, V. Bansal, Identifying trends in gold nanoparticle toxicity and uptake: size, shape, capping ligand, and biological corona, ACS Omega 4 (2019) 242–256.
[46] A. Woźniak, A. Malankowska, G. Nowaczyk, B.F. Grześkowiak, K. Tuśnio, R. Słomski, A. Zaleska-Medynska, S. Jurga, Size and shape-dependent cytotoxicity profile of gold nanoparticles for biomedical applications, J. Mater. Sci.: Mater. Med. 28 (2017) 1–11.
[47] J. Stabile, D. Najafali, Y. Cheema, C.T. Inglut, B.J. Liang, S. Vaja, A.J. Sorrin, H.-C. Huang, Engineering gold nanoparticles for photothermal therapy, surgery, and imaging, Nanoparticles for biomedical applications, Elsevier2020, pp. 175–193.
[48] G. Sun, T. Fan, L. Zhao, Y. Zhou, R. Zhong, The potential of combi-molecules with DNA-damaging function as anticancer agents, Future Med. Chem. 9 (2017) 403–435.